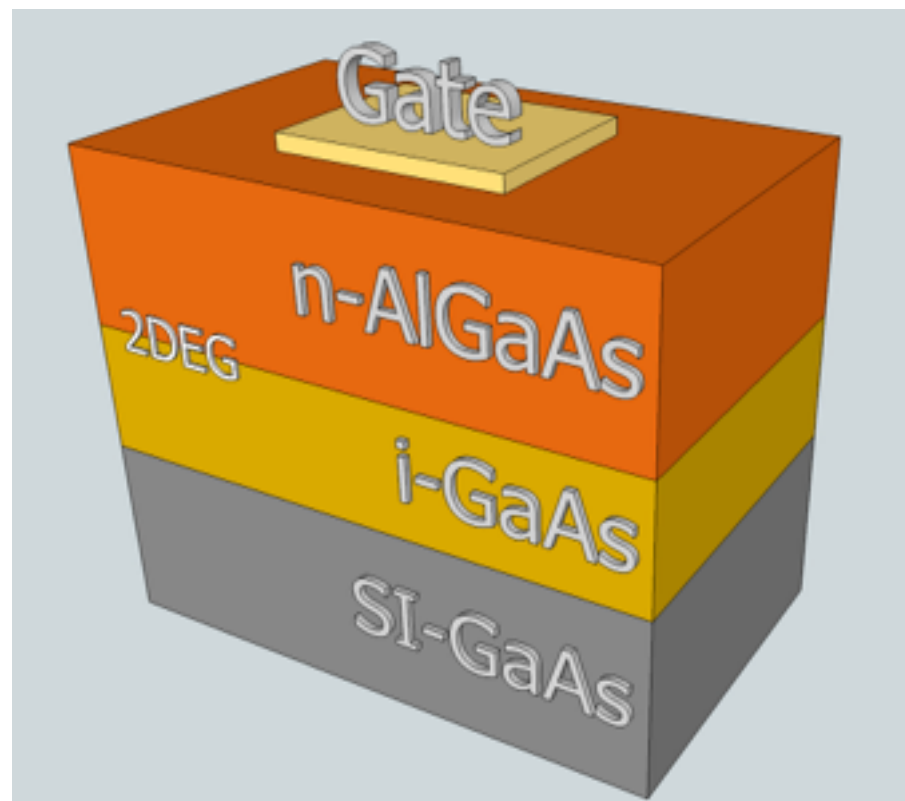


2DEG in GaAs/GaAlAs heterostructures



$$\sigma_0 = n\mu e$$

$$v = \mu E$$

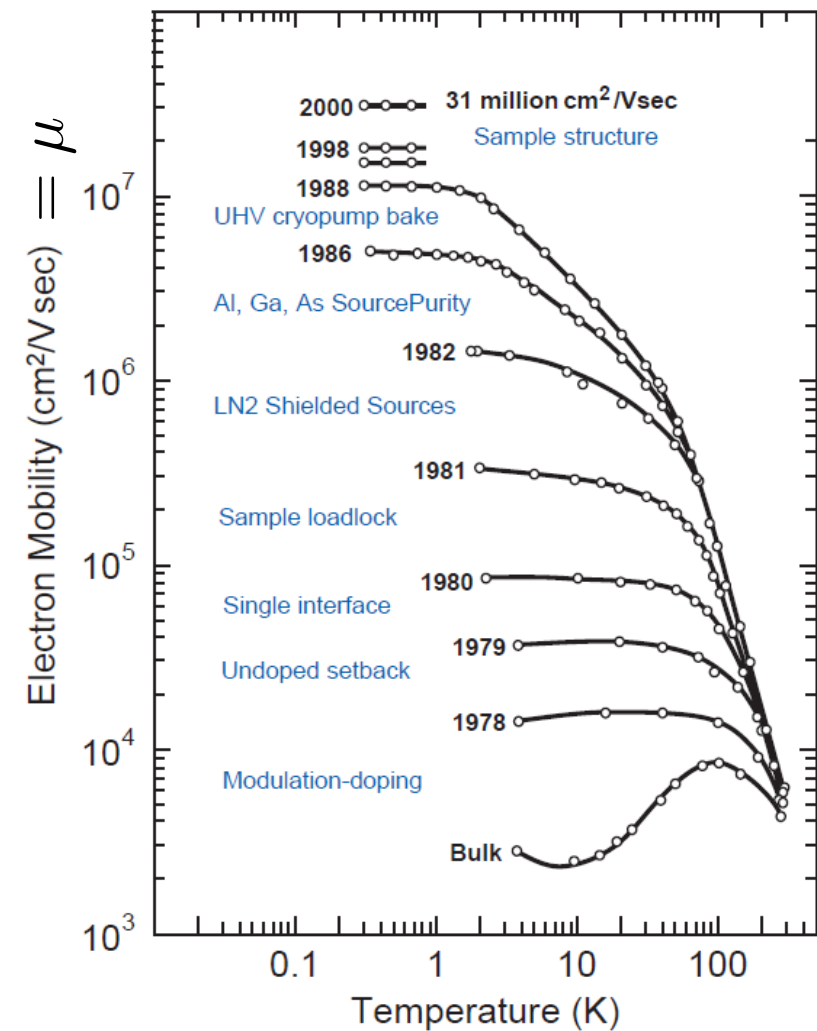
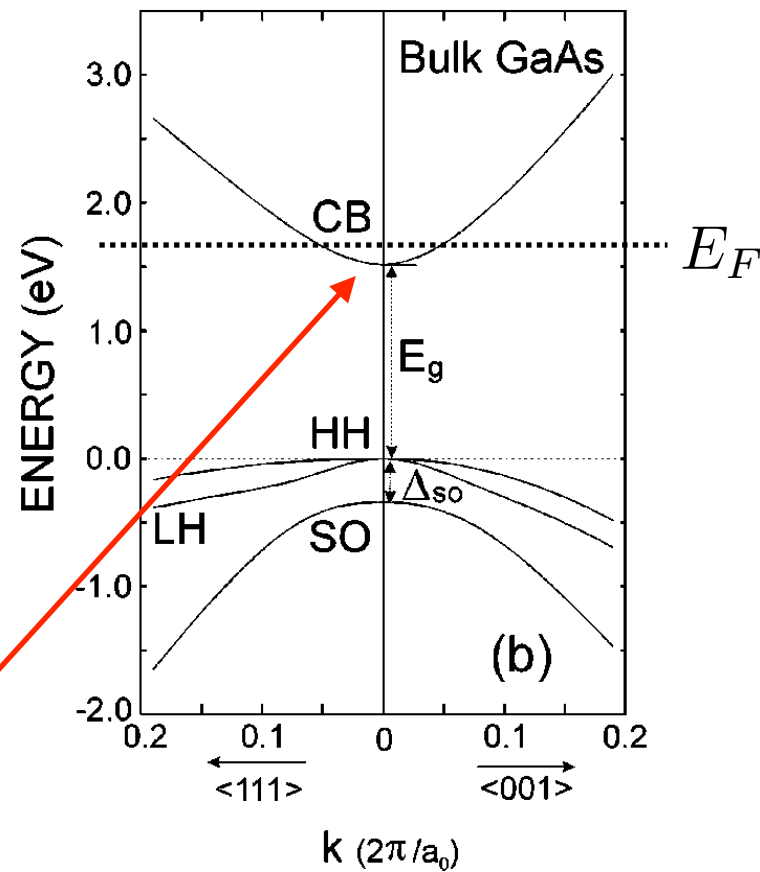


Figure 2. History of improvements in the mobility of 2DEG in GaAs-AlGaAs heterostructure. Adapted from [6].

n-doped GaAs

- “free” electrons with effective mass m^*
- envelope-function appr.

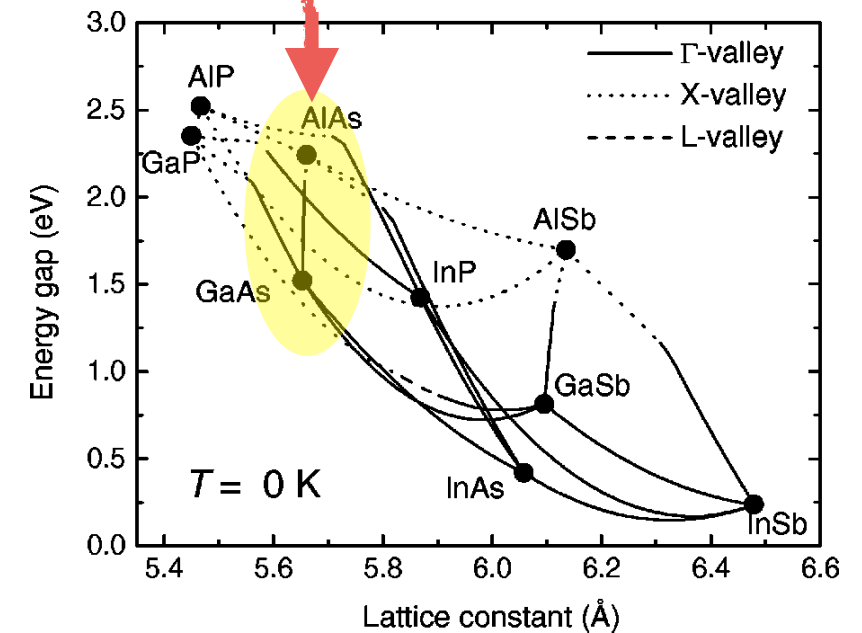


conduction band edge

conduction band

gap

valence band



Quantised conductance in a Quantum Point Contact (QPC)

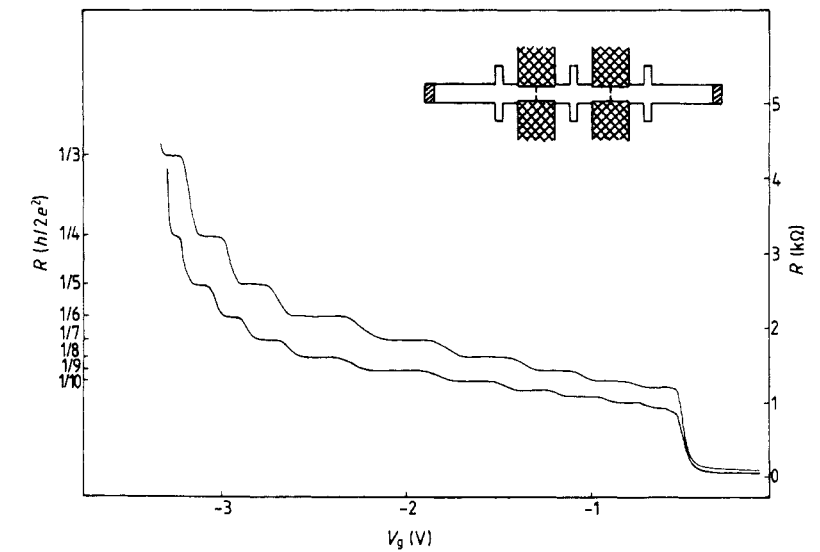
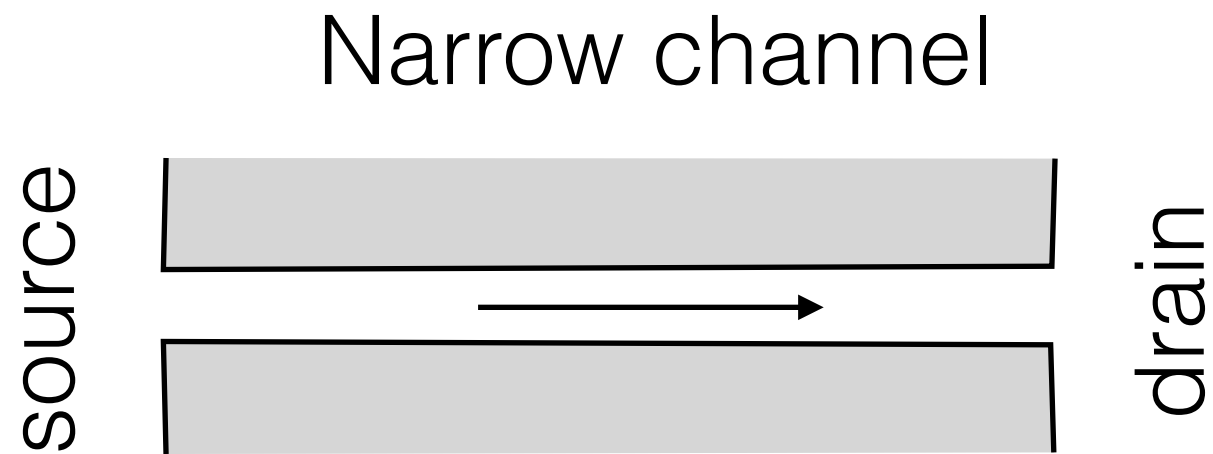


Figure 1. The channel resistance at $T \sim 0.1$ K is plotted as a function of gate voltage for two different carrier concentrations induced by illumination. The existence of a resistance quantised in units of $h/2ie^2$, where i is the number of occupied sub-bands, is illustrated. The inset shows a schematic diagram of the device used in this work. The split gate itself is $0.5 \mu\text{m}$ wide and $0.4 \mu\text{m}$ long. Two split gates are illustrated, one of which is selected for the experiment.

Quantised conductance in a Quantum Point Contact (QPC)

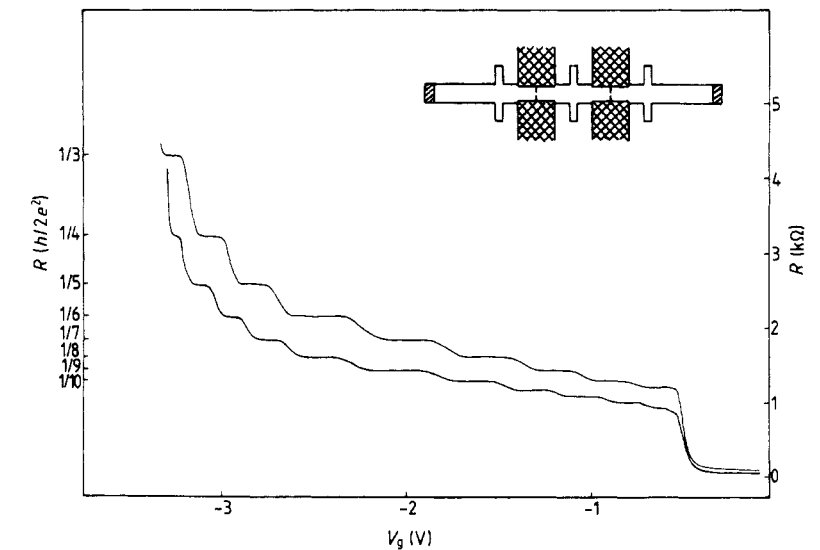
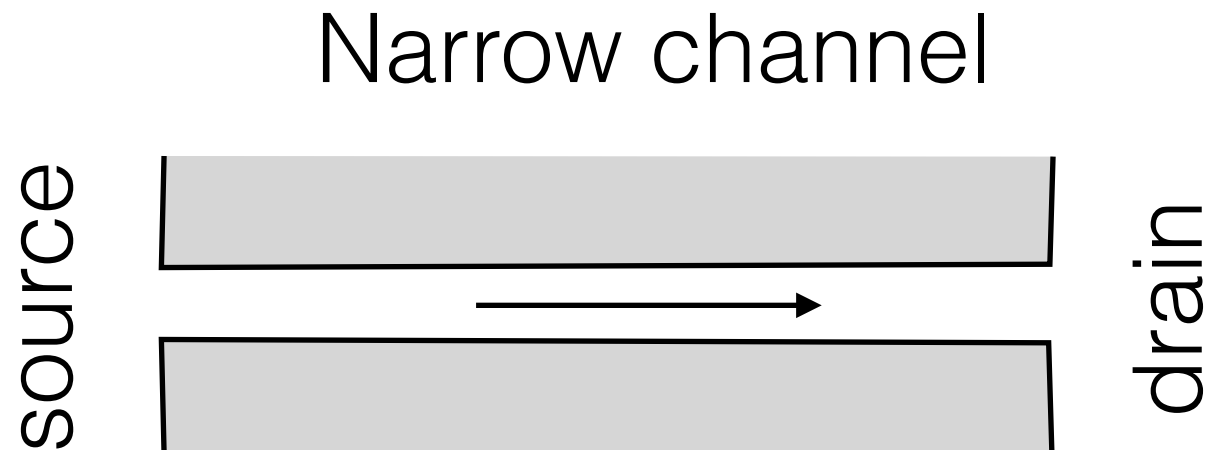


Figure 1. The channel resistance at $T \sim 0.1$ K is plotted as a function of gate voltage for two different carrier concentrations induced by illumination. The existence of a resistance quantised in units of $h/2ie^2$, where i is the number of occupied sub-bands, is illustrated. The inset shows a schematic diagram of the device used in this work. The split gate itself is $0.5 \mu\text{m}$ wide and $0.4 \mu\text{m}$ long. Two split gates are illustrated, one of which is selected for the experiment.

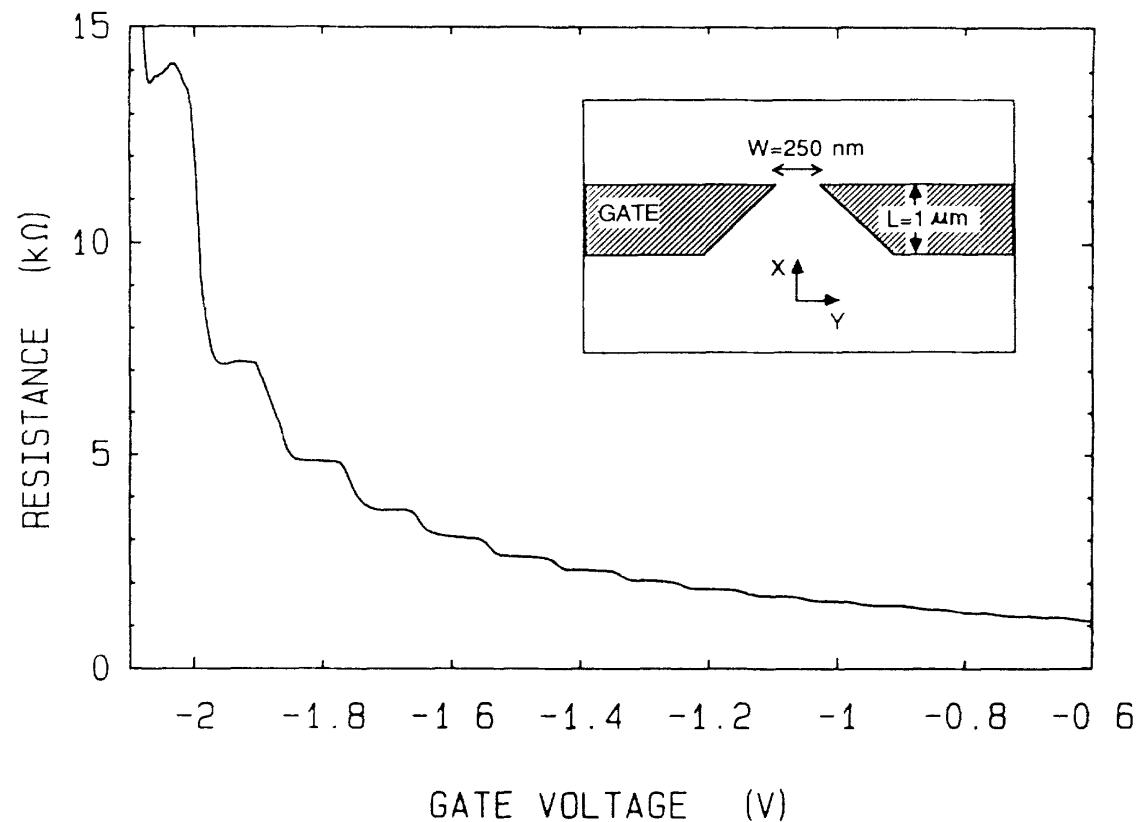


FIG. 1. Point-contact resistance as a function of gate voltage at 0.6 K. Inset: Point-contact layout.

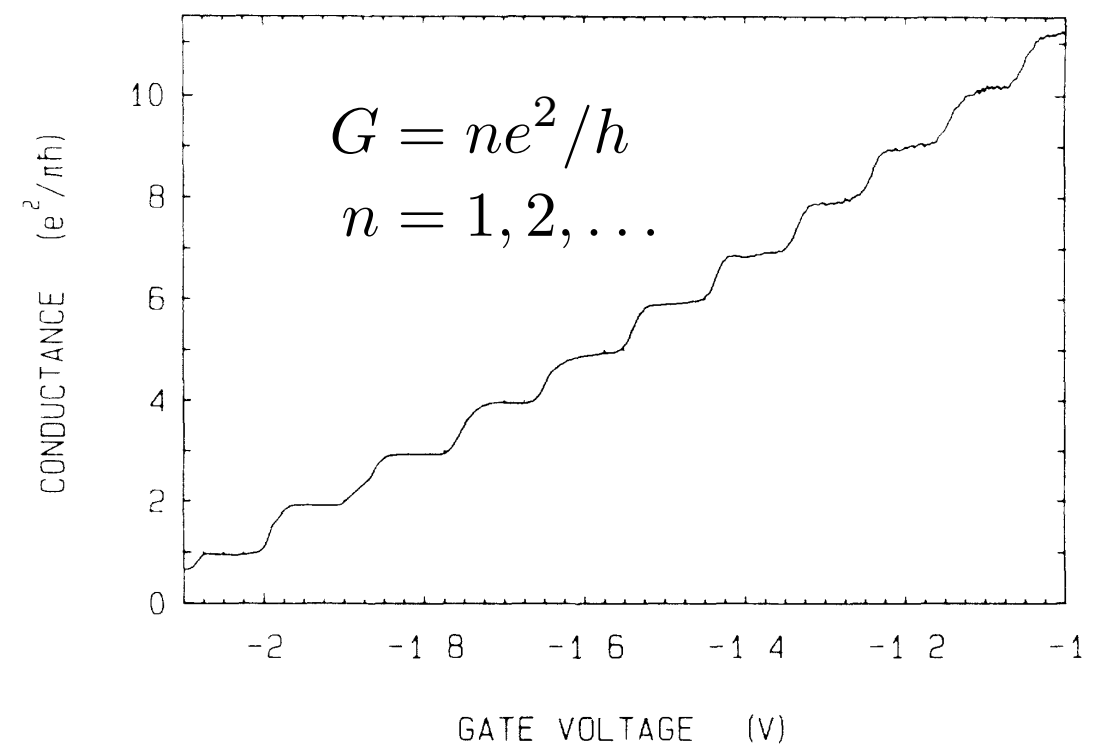


FIG. 2. Point-contact conductance as a function of gate voltage, obtained from the data of Fig. 1 after subtraction of the lead resistance. The conductance shows plateaus at multiples of $e^2/\pi\hbar$.

Quantised conductance of a carbon nanotube (CNT)

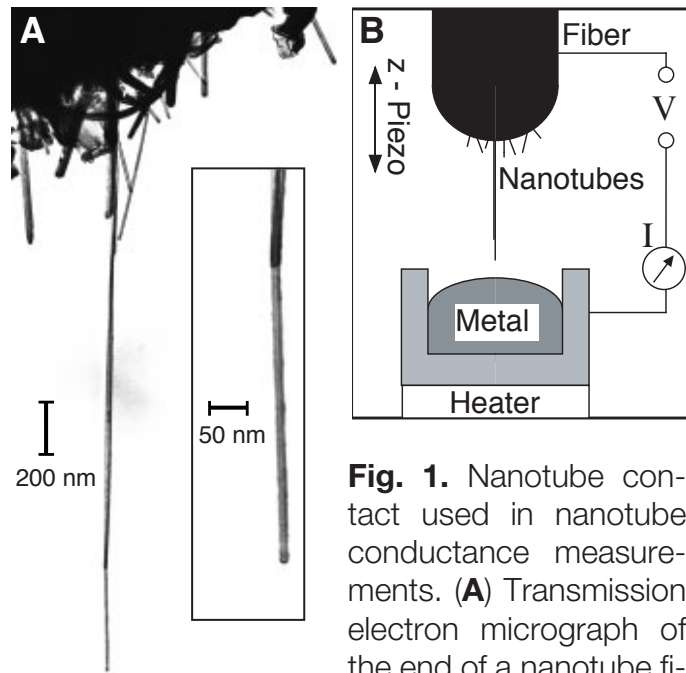
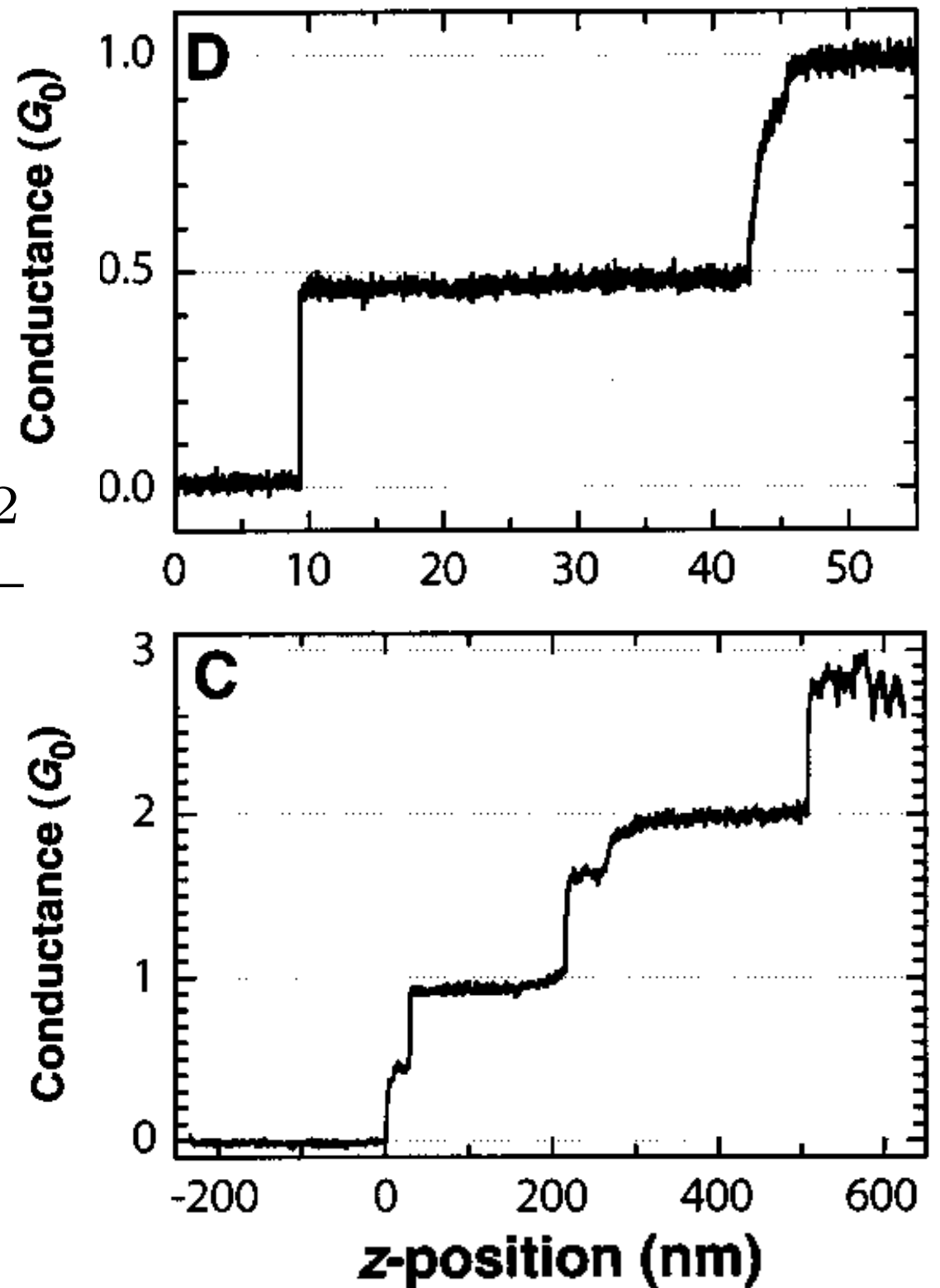


Fig. 1. Nanotube contact used in nanotube conductance measurements. **(A)** Transmission electron micrograph of the end of a nanotube fiber recovered from the nanotube arc deposit. The fibers consist of carbon nanotubes and small graphitic particles. The fiber shown here is ~1 mm long and 0.05 mm at the tip, from which protrude several long and straight nanotubes. The nanotubes are very clean after they have been dipped in liquid metal (like the one shown), in contrast to the virgin tips on which many small graphitic particles are seen. The long nanotube is 2.2 μm long and 14 nm wide. The inset shows the end of the longest tube under higher magnification; it is bundled together with another one that terminates 400 nm before the first one. **(B)** Schematic diagram of the experimental setup. The nanotube contact is lowered under SPM control to a liquid metal surface. After contact is established, the current I is measured as the fiber is moved into the liquid metal, so that the conductance can be determined as a function of the position of the nanotube contact.

The fibers consist of carbon nanotubes and small graphitic particles. The fiber shown here is ~1 mm long and 0.05 mm at the tip, from which protrude several long and straight nanotubes. The nanotubes are very clean after they have been dipped in liquid metal (like the one shown), in contrast to the virgin tips on which many small graphitic particles are seen. The long nanotube is 2.2 μm long and 14 nm wide. The inset shows the end of the longest tube under higher magnification; it is bundled together with another one that terminates 400 nm before the first one.

$$G_0 = \frac{2e^2}{h}$$



Four-terminal measurement on a quasi 1D channel

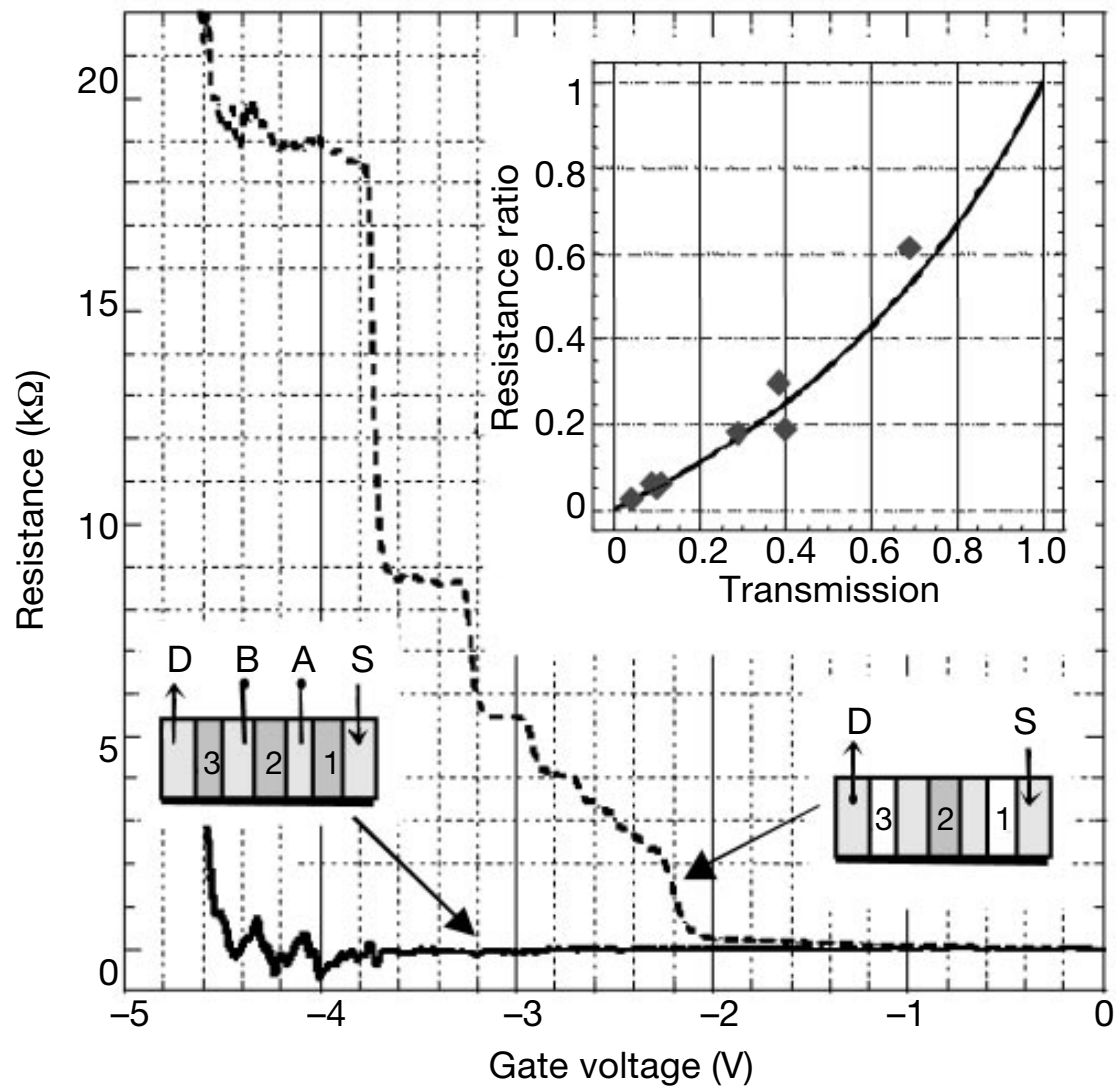
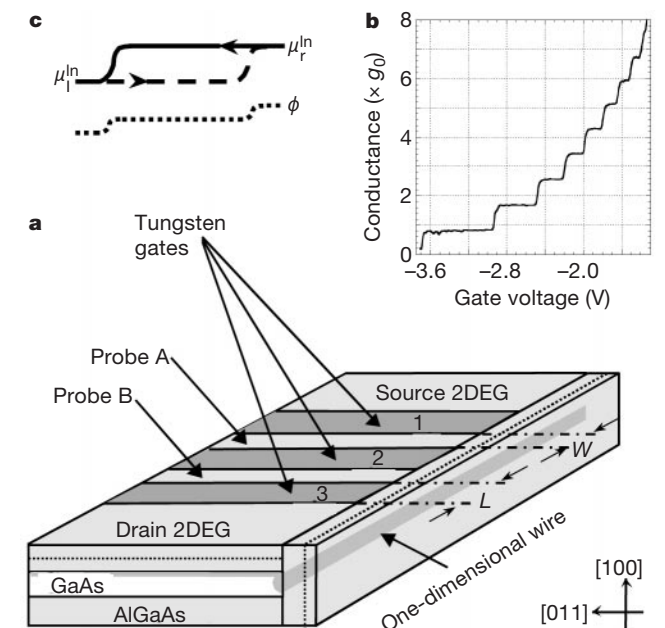


Figure 2 Two- and four-terminal resistances of a ballistic quantum wire. The dashed line shows the two-terminal resistance of the 2- μm -long central section of the wire versus the voltage applied to the associated gate 2. Gates 1 and 3 are not activated. The solid line shows the four-terminal resistance, $(V_A - V_B)/I$, versus the voltage applied to gate 2. Here V_A and V_B are the voltages at probes A and B respectively and I is the current driven from source to drain. For this measurement, the voltages applied to gates 1 and 3 correspond to a single mode in the wire sections in front of these gates. Measurements were performed at a temperature of $\theta = 300$ mK with an excitation current smaller than 1 nA. While the two-terminal resistance moves through the characteristic quantized resistance steps, the four-terminal resistance fluctuates around zero indicating that the inherent resistance of a clean one-dimensional wire is vanishingly small. The small oscillations around zero resistance (from -3.8 V to -4.5 V) suggest that mesoscopic variation of the various transmission amplitudes with the one-dimensional density dominate the resistance in this regime. Indeed a similar, although not identical, pattern is observed upon successive cool-downs of the same device. As expected, similar mesoscopic variations are observed when a magnetic field is applied (see Fig. 3). Inset, probe invasiveness in a quantum wire. Diamonds, the ratio between the four-terminal and two-terminal resistances versus the invasiveness of the voltage probes (see text). Solid line, theoretical prediction of the Landauer-Buttiker model¹⁶ (see text). All measurements are for single-mode wires.

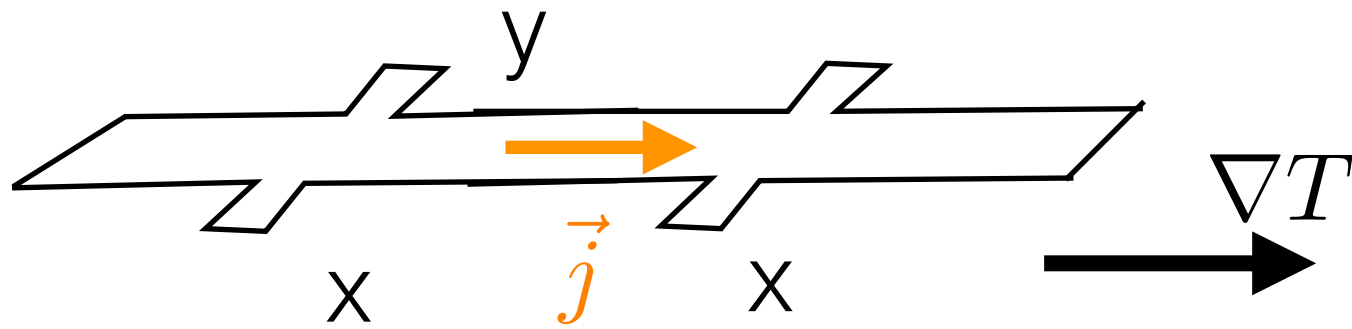
$$G = \mathcal{T} \frac{e^2}{h} \quad (\text{Landauer-Buttiker})$$

$$\mathcal{T} + \mathcal{R} = 1$$

$$R = 1/G = \frac{h}{e^2} + \frac{h}{e^2} \frac{\mathcal{R}}{\mathcal{T}}$$



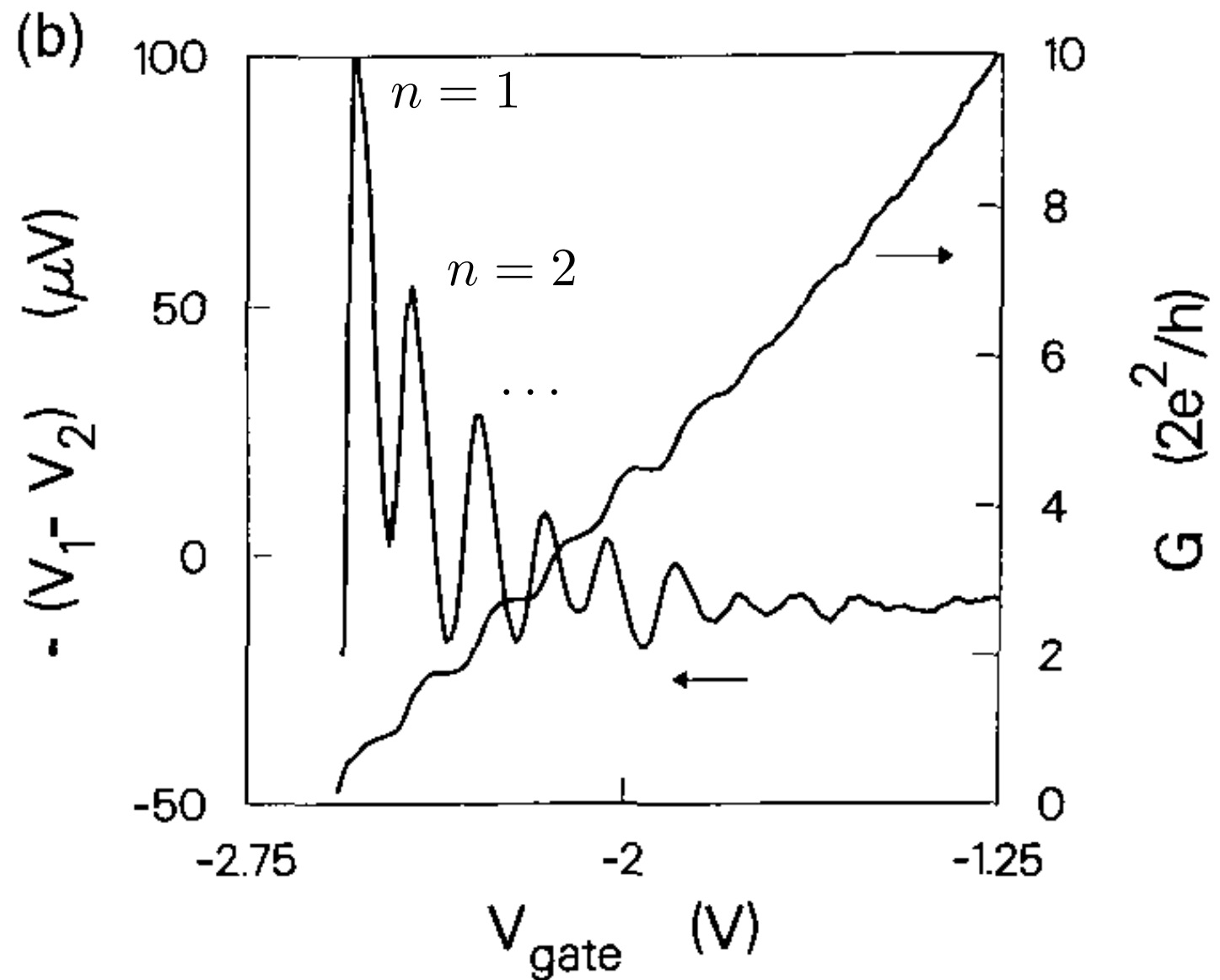
Thermopower



Seebeck and Peltier effects

- conductance quantised in QPC
- thermopower (Seebeck coefficient) oscillates, maxima reach

$$S_{max} = \frac{k}{e} \frac{\ln 2}{n + \frac{1}{2}}$$



Quantum dots (QDs)

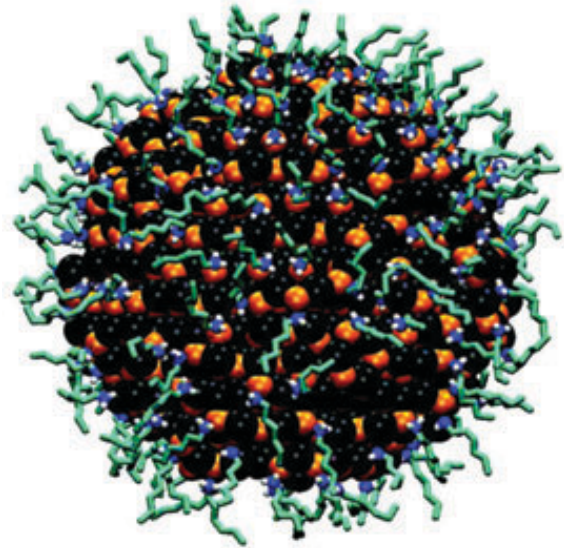
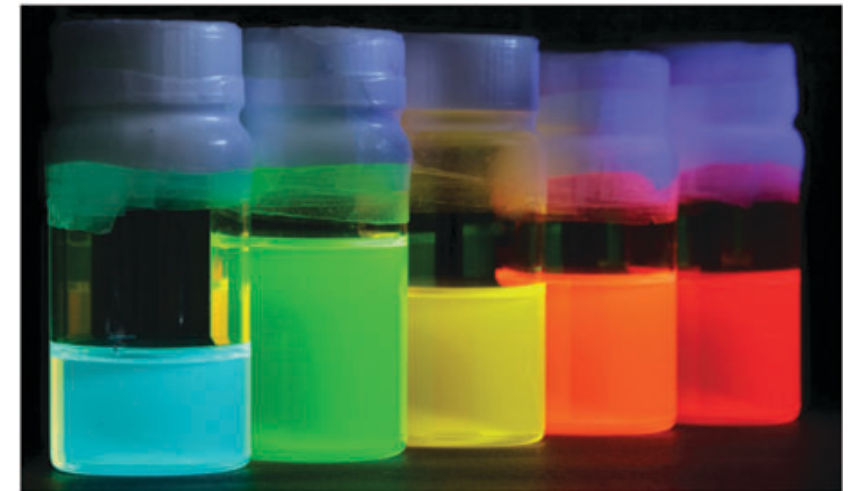


Fig. 2 Molecular simulation snapshot of a colloidal CdSe NC capped by hexylamine molecules. Colour coding: black, Se; orange, Cd; light blue, C; dark blue, N; white, H; yellow, S; brown, P; red, O. The simulation methodology is described in ref. 3. Courtesy of P. Schapotschnikow (Delft University of Technology, Netherlands).



Colloidal CdSe nanocrystals (NC), diameter 1.7-4.5 nm (left to right) under UV illumination.

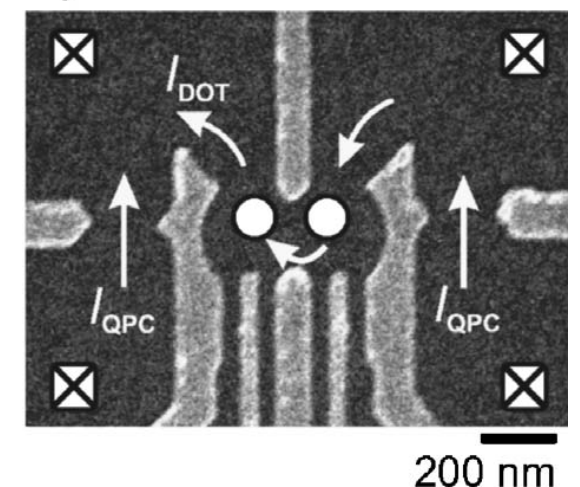
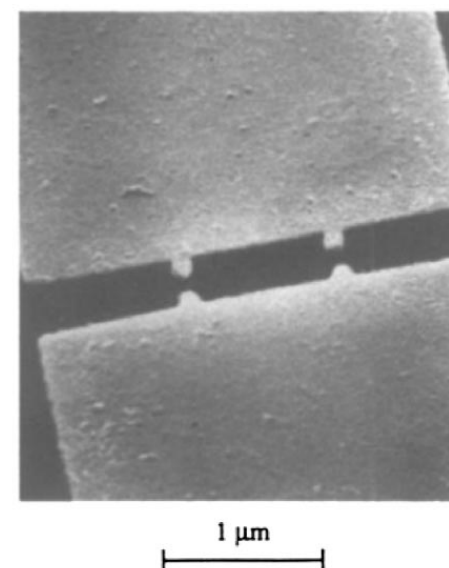
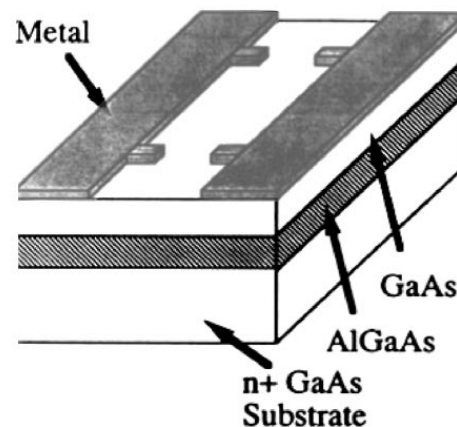
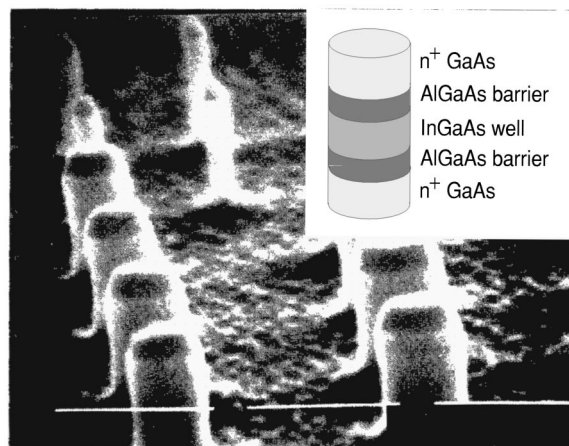
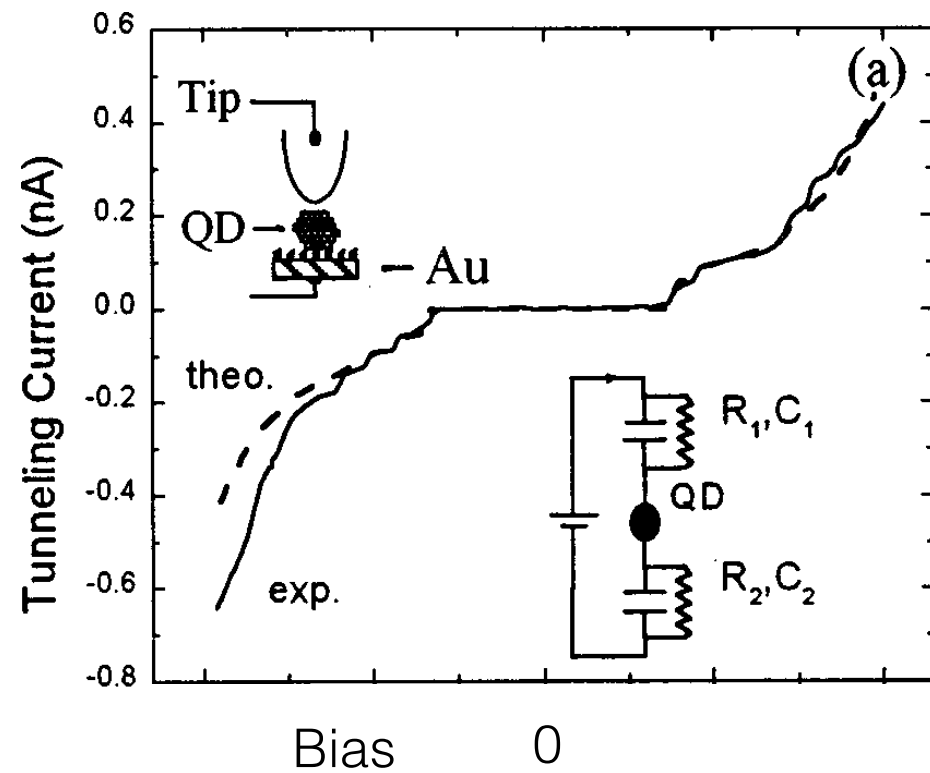


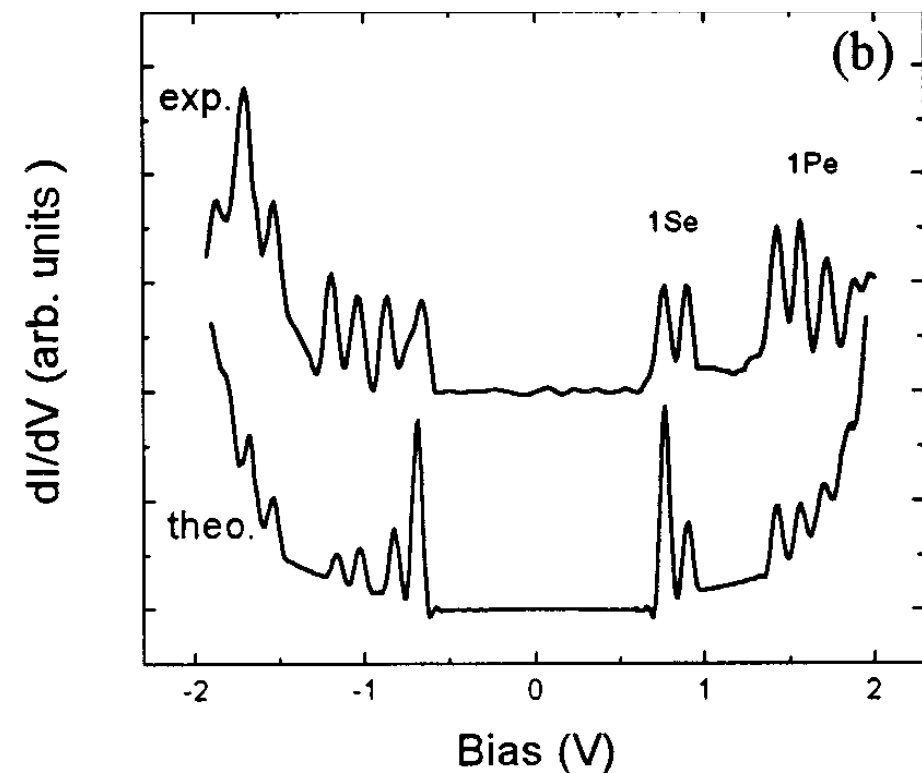
FIG. 4. Scanning electron micrograph showing etched quantum dots. (The white bars have a length of 0.5 μm.) Inset, schematic picture of a single dot structure. After Reed *et al.*, 1988.

Tunneling current: tip-QD-substrate



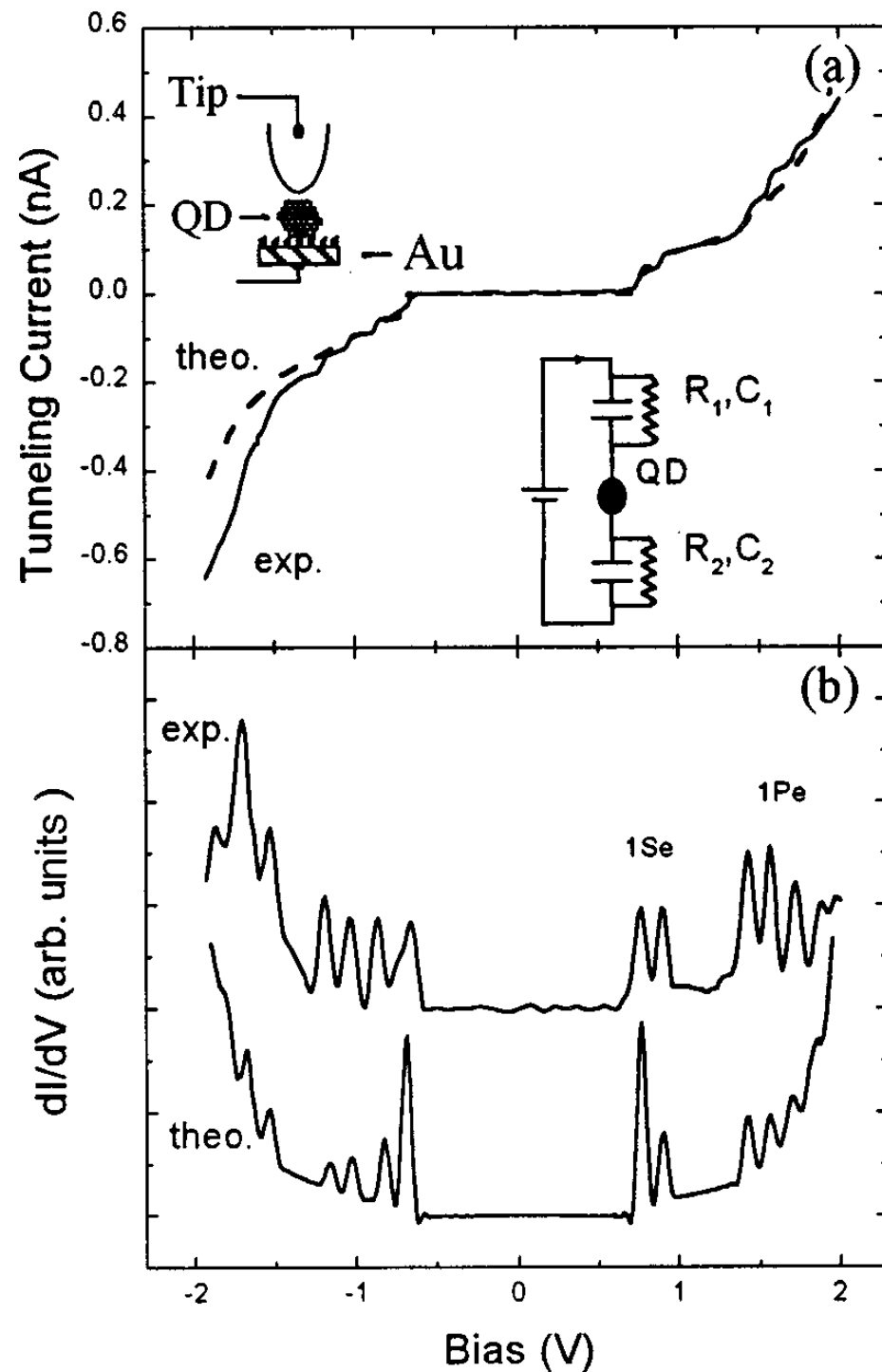
- non-linear VA characteristics
- clear steps visible at certain voltages
- InAs QD, diameter 4.4 nm

Differential conductivity - energy level spectroscopy

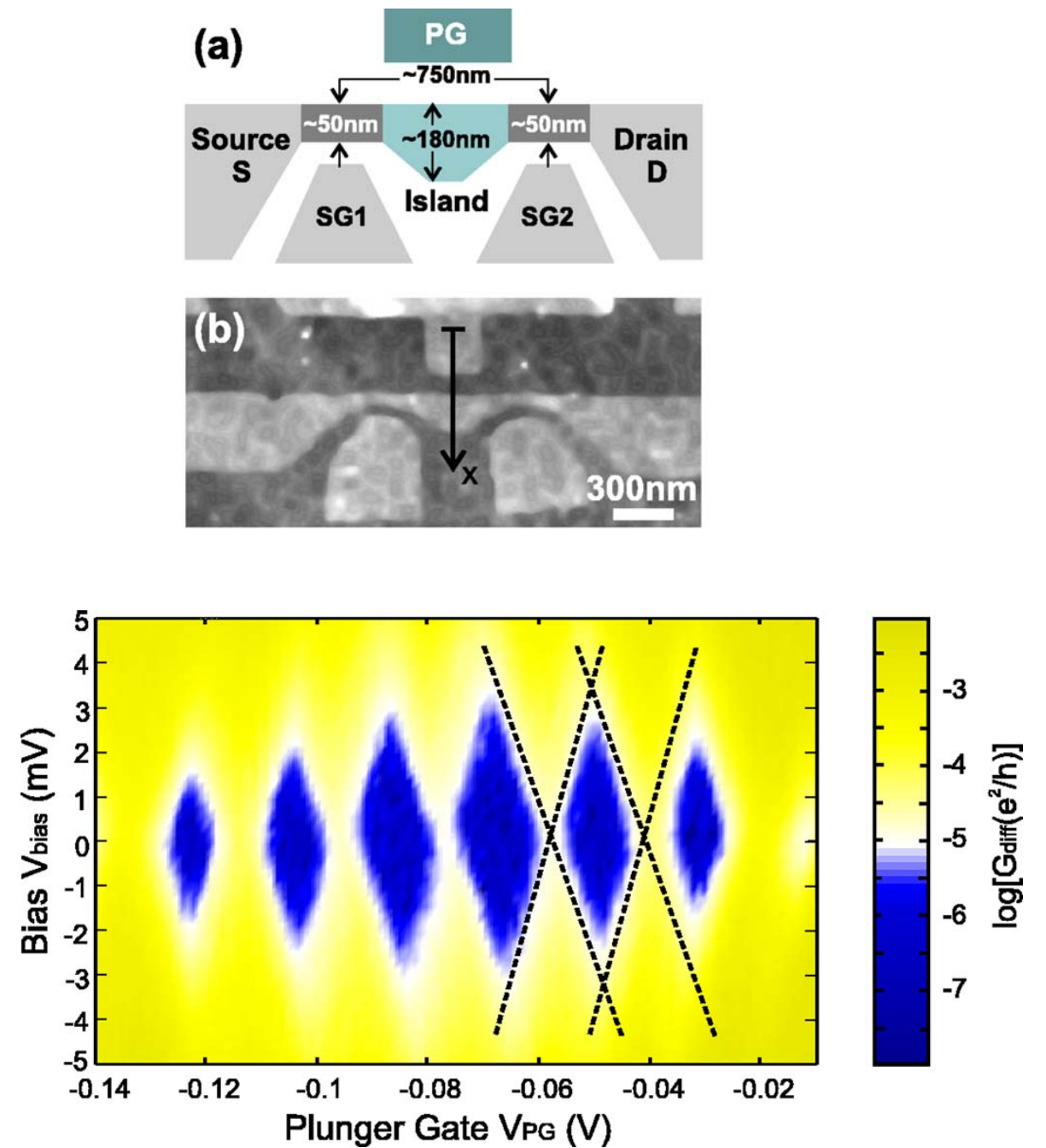


Tunneling through quantum dots

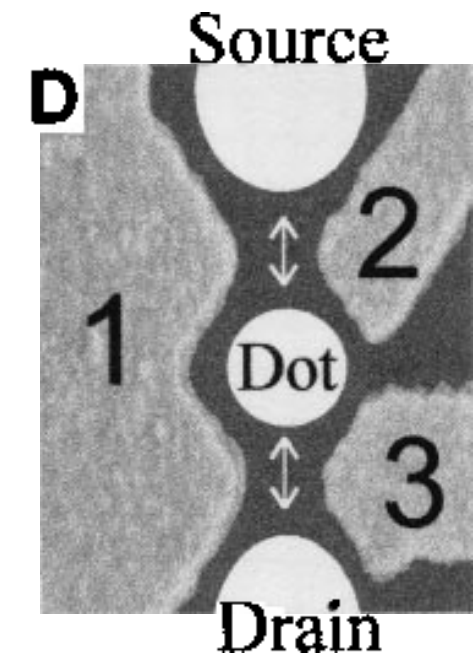
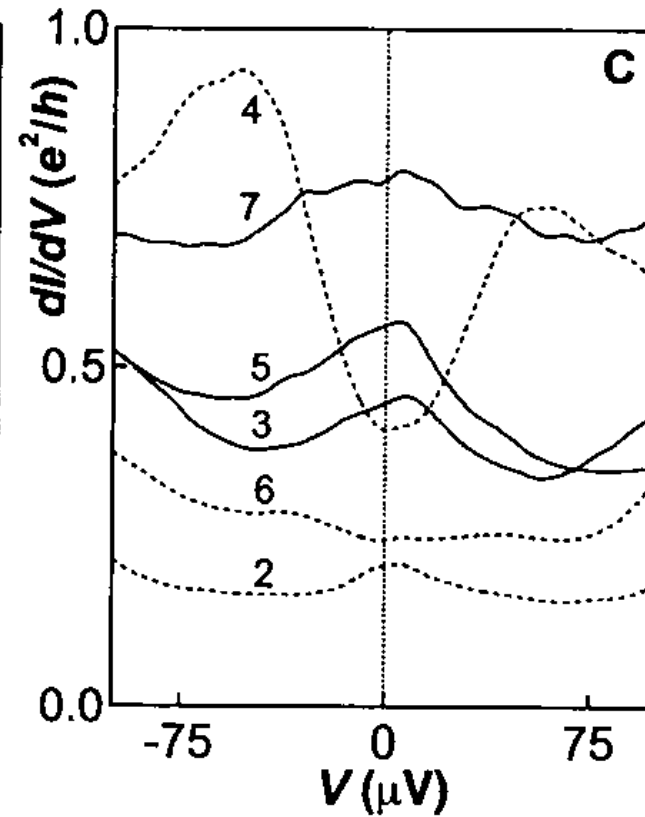
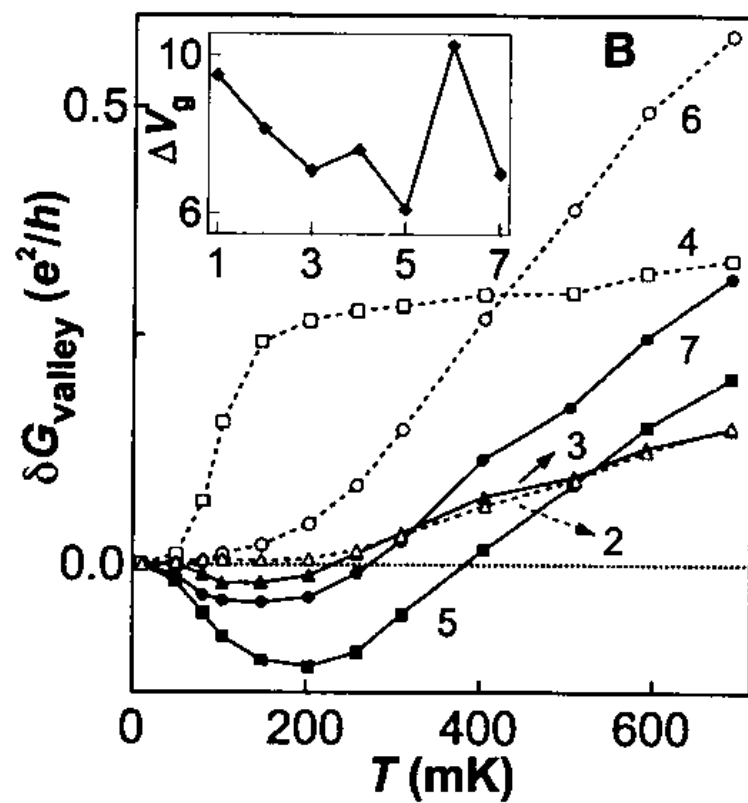
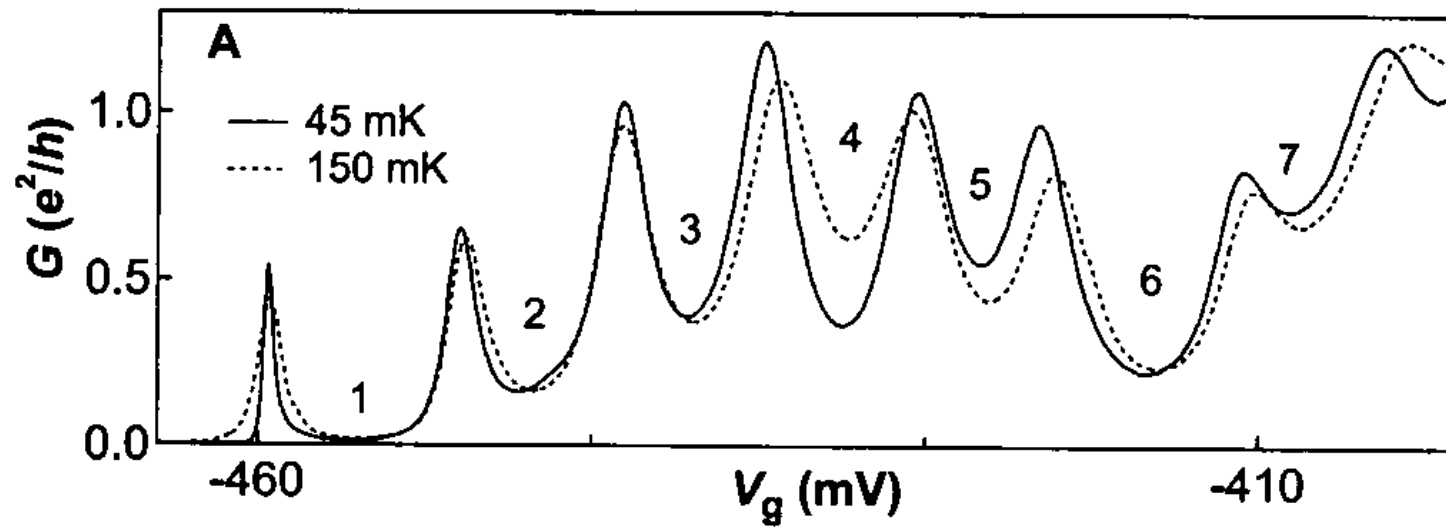
Small dots - resonant tunneling



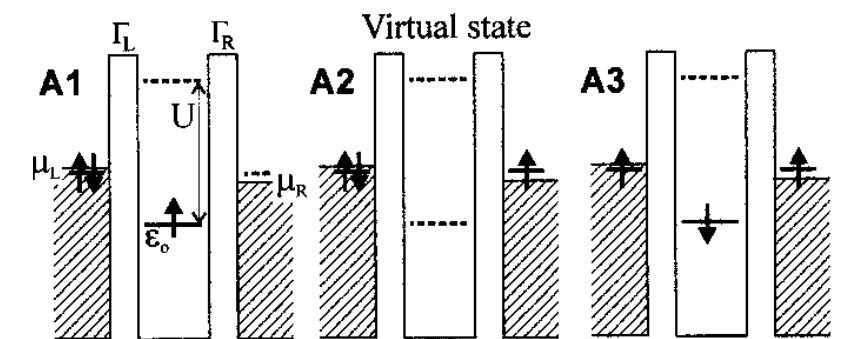
Larger dots - Coulomb blockade



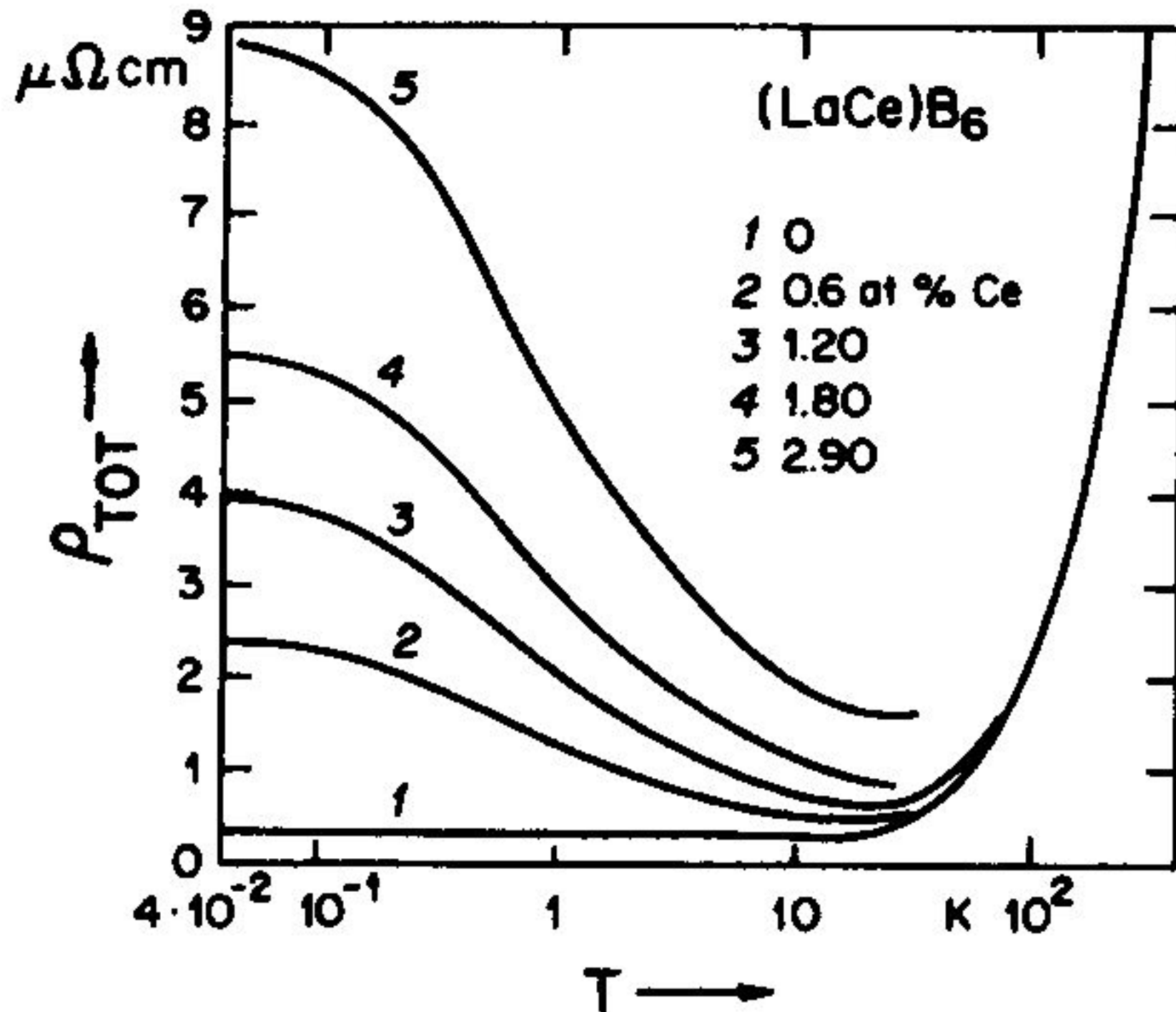
Kondo effect in a quantum dot



- 2DEG with gates
- more complicated transport scenario



Kondo effect - the original



Kondo temperature:

$$T_K = \frac{D}{k_B} \exp(-D/2|J|)$$

coupling between
conduction electron
spin and impurity
spin:

$$\hat{H}_{ex} = -J\vec{S} \cdot \hat{s}$$

Kondo effect in a quantum dot

